International Journal of Solid Materials
Vol. 1, Issue 1, 2019, Pages 27-49
Published Online on January 31, 2019

http://jyotiacademicpress.org

FAILURE ANALYSIS OF REINFORCED CONCRETE BEAMS IN BENDING STRENGTHENED WITH CFRP BY USING FINITE ELEMENT METHOD AND EXPERIMENTAL TESTS

MOHSEN FOROUZANMEHR[1], KAZEM REZA-KASHYZADEH[2], KHASHAYAR BAZIARI[3] and MEHRDAD MOHAMMADI[3]

[1]School of Mechanical Engineering
Sharif University of Technology
International Branch
Kish Island
Iran
e-mail: m_forouzanmehr@kish.sharif.edu

[2]Laboratory Head
Mechanical Characteristics Lab
Center for Lab Services
Sharif University of Technology
Tehran
Iran
e-mail: Kazem.kashyzadeh@gmail.com
k_kashyzadeh@mehr.sharif.edu

Keywords and phrases: reinforced concrete beam, damage plasticity model, failure analysis, CFRP.
Received October 2, 2018; Revised November 11, 2018; Accepted December 10, 2018

[3]School of Mechanical Engineering
Islamic Azad University
Shiraz Branch
Shiraz
Iran
e-mail: khashayarbaziari@yahoo.com
mehr4457@gmail.com
mohammadi_mehrdad@iaushiraz.ac.ir

Abstract

The main aim of this research is to study the structural behaviour of reinforced concrete beam strengthened in bending with carbon fiber reinforced polymer (CFRP). The three groups of CFRP-strengthened beams with different loading conditions were simulated and analyzed by using finite element method. The obtained results in each group were compared with experimental data. The curves of load vs. mid-span displacement were plotted for all types of CFRP beams. It was shown that there are good agreements between experimental data and the FE results. The numerical failure modes were matched with non-shear beams which are demonstrated tension and compressive modes in terms of plasticity failure. The present simulation can be used as a practical work in civil and mechanical engineering for these types of materials which are used to increase the strength of concrete beams.

1. Introduction

The use of fiber reinforced polymers (FRPs) in concrete structures develops for different purposes. The FRP can improve some properties of the material. But, failure of these structures due to various loadings such as cyclic, vibration and static loading is one of the most significant challenges in mechanical and civil engineering [2, 3]. The use of carbon fiber reinforced polymer (CFRP) beams is commonly known for structures that are used in practical applications to increase the strength and to prevent failure [4]. Several experimental and numerical investigations have been carried out in the design and construction of the structures made of CFRP materials [5-8]. Some laboratory standard tests have been used to determine the failure resistance of CFRP materials [1].

Jiang and Chorzepa [7] have proposed an effective numerical methodology to predict the impact response of pre-stressed concrete members. Khshain et al. [8] and Hognestad [9] have reported the mechanical behaviour of the concrete. Drucker-Prager hypothesis is one of the strong hypotheses that extensively is used for concrete. A cone is assumed as the boundary surface and the failure is determined by strain energy. The model of concrete damaged plasticity (CDP) can be used as modified Drucker-Prager [10].

Three parameters are necessity for finite element simulation of the CDP model. The first parameter is eccentricity which can calculate as the ratio of tensile to compressive strength. The second parameter is the ratio of biaxial to uniaxial strength. And the last parameter is the dilation angle which is used to characterize the concrete performance under compound stress [10].

In the present paper, the reinforced concrete beam in bending strengthened with CFRP was simulated. It was assumed that the structure has four layers. The substrate layer consisted of concrete (a mixture of concrete and steel) [6]. The first and second layers were considered CFRP and adhesive, respectively [1]. Then, the failure analyze was done by utilizing Hashin theory [12, 13].

2. Finite Element Modelling

The three specimens (CFRP) with different dimensions were used to study the failure and strength of structures. All models include concrete, steel bars and CFRP layer. The location of the installed CFRP sheets under the reinforced concrete beams are shown in Figure 1. Geometric sizes of the beams are reported in Table 1.

Table 1. Geometric dimensions of the different specimens

Sample	Dimension	Width (mm)	Depth (mm)	Length (mm)
A		115	146	1500
B		230	292	3000
C		368	467	4800

The thickness of CFRP and adhesive layer were considered equal to 0.165 and 0.636mm, respectively. These beams were assumed without any defects such as a notch, crack in order to predict strength and bending failure.

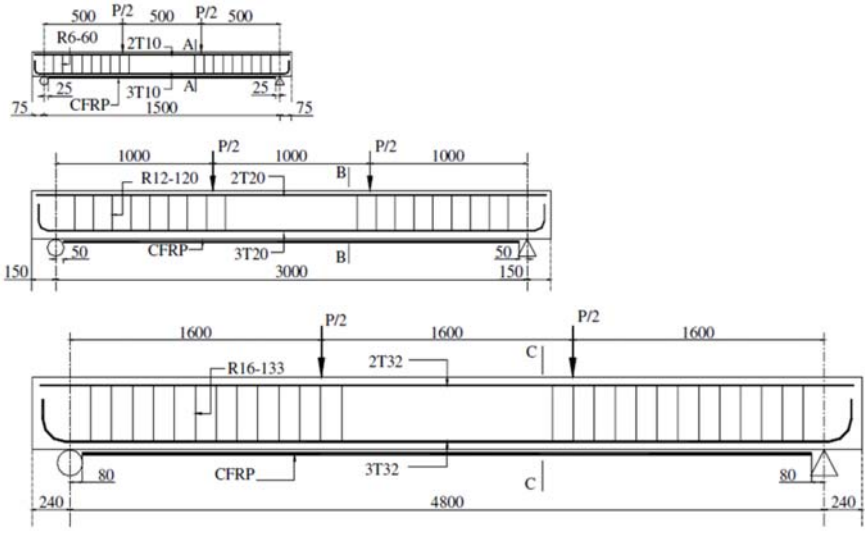

Figure 1. The geometry and specimen reinforcing details for beams of series A, B, and C (all dimensions are in mm).

The steel rods with the diameter of 60, 120, and 133mm were used for three different beams. The concrete dimensions and exact location of rods in the cross sections of reinforced concrete beams are demonstrated in Figure 2.

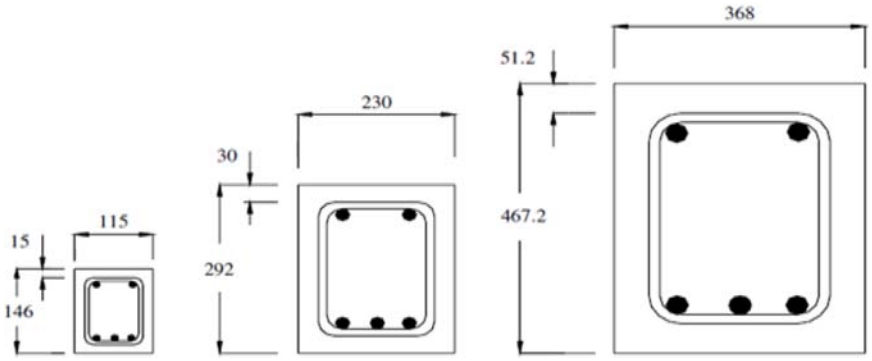

Figure 2. The detail of cross sections for beam series of A, B, and C.

Faggiani et al. [14] and Shi et al. [15] have showed that the SC8R element (8-node quadrilateral continuum shell element) is suitable for simulating CFRP and adhesive layers separately.

In this study, adhesive layers were used as interface elements between the reinforced concrete beam and CFRP layers. The 8-node 3-D cohesive element (COH3D8) was used to model the adhesive zone. Finally, concrete and steel were modelled using an 8-node linear brick element with reduced integration (C3D8R) and truss elements, respectively. Two rigid bodies were used as the jaw for loading are illustrated in Figure 3.

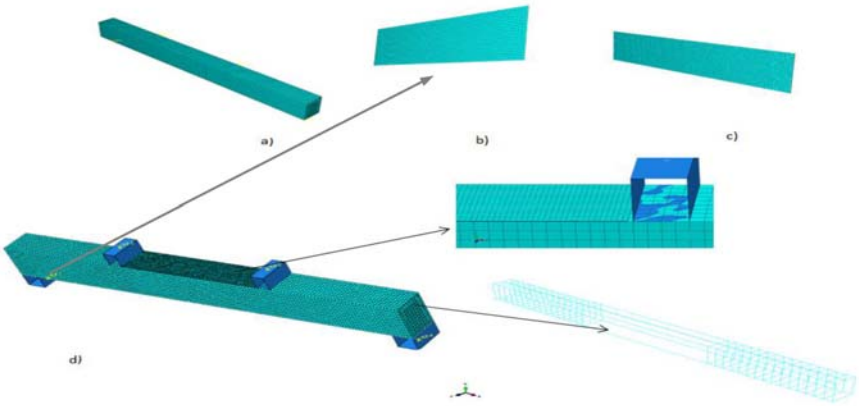

Figure 3. All parts of the finite element model: (a) concrete beam (solid elements), (b) CFRP layer (shell elements), (c) the adhesive layer (COH3D8 elements), and (d) CFRP beams with the location of CFRP, adhesive and steel (truss elements).

2.1. Contact modelling and mesh convergence

Selecting the proper mesh size of the FEM is one of the important factors to simulate the behaviour of materials exactly. In this regard, mesh convergence was studied on the all parts of the model separately. Fine meshes were used to simulate the contact zone and coarse meshes were used away from the contact trace of loading. A friction coefficient of

0.364 was used between the CFRP, adhesive and concrete surfaces [15, 16]. The simple boundary conditions on one side and the roller bending on the other side [1] were applied by using rectangular rigid bodies. Two rectangular rigid parts were defined at the top of the specimens as the loading jaw. The loads were applied to the reference points $(RP_i,\ i = 1, 2)$. These points were tied on the beam. In the reference points, all degrees of freedom except for vertical displacements were restricted. The simple B.Cs (i.e., $U_1 = U_2 = 0, UR_3 = 0$) for both sides of the beam and roller bending boundary conditions (i.e., $U_2 = 0, UR_3 = 0$) were considered. The static loading and vertical displacement were considered at points 3 and 4. The general schematic of the FE model of CFRP beam with reference points is displayed in Figure 4.

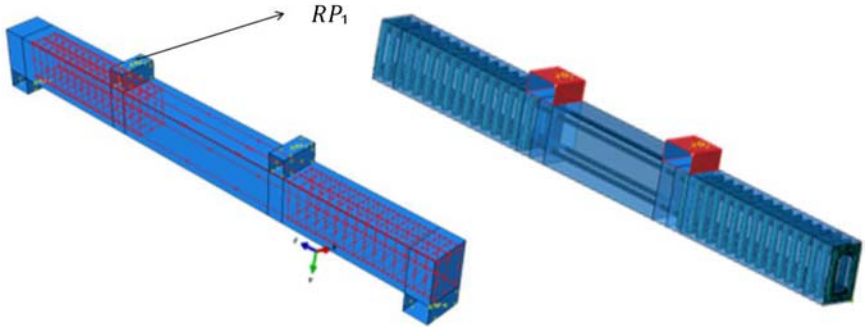

(a) (b)

Figure 4. (a) A model of CFRP beam in ABAQUS and internal sections with reference points, (b) CFRP model with an internal section.

2.2. Damage plasticity model of concrete

The FE model was considered pure bending without any shear reinforcement. Lee and Fenves [17] have proposed a yield function as following:

$$F = \frac{1}{1-\alpha}\left(\bar{q} - 3\alpha\bar{p} + \beta(\tilde{\varepsilon}^{pl})\langle\hat{\bar{\sigma}}_{\max}\rangle - \gamma\langle -\hat{\bar{\sigma}}_{\max}\rangle\right) - \bar{\sigma}_c(\tilde{\varepsilon}_c^{pl}). \qquad (1)$$

In which, parameter α is calculated as:

$$\alpha = \frac{\left(\frac{\sigma_{b0}}{\sigma_{c0}}\right) - 1}{2\left(\frac{\sigma_{b0}}{\sigma_{c0}}\right) - 1}, \tag{2}$$

where σ_{b0} is the biaxial compressive strength and σ_{c0} is the uniaxial stress. It is necessary to define the ratio of $\sigma_{b0} / \sigma_{c0}$ for finite element simulation. It is approximately equal to 1.16 [17]. Related to the Equation (1), $\overline{p}$ is the hydrostatic pressure and $\overline{q}$ is the equivalent effective Von Misses stress, $\beta\left(\overline{\epsilon}^{pl}\right)$ is the yield function. If the maximum quantity of principal effective stress is considered positive, the yield function can be written as follows:

$$\beta\left(\overline{\epsilon}^{pl}\right) = \frac{\overline{\sigma}_c(\tilde{\epsilon}_c^{pl})}{\overline{\sigma}_t(\tilde{\epsilon}_t^{pl})}(1 - \alpha) - (1 + \alpha), \tag{3}$$

where $\overline{\sigma}_c(\tilde{\epsilon}_c^{pl})$ and $\overline{\sigma}_t(\tilde{\epsilon}_t^{pl})$ are the stress under compression and tension loading, respectively. In the biaxial state, when $\hat{\overline{\sigma}}_{\max} = 0$, the yield function is equal to zero and only remained parameter is α.

Another parameter is the yield surface that is defined by the parameter γ. It is given in Equation (4).

$$\gamma = \frac{3(1 - K_c)}{2K_c - 1}, \tag{4}$$

where K_C is the ratio of the tensile to the compressive stresses in the meridian lines (Figure 5). The ratio of $K_C = 2/3$ and 1 are related to the Rankine and Drucker-Prager criteria, respectively [10].

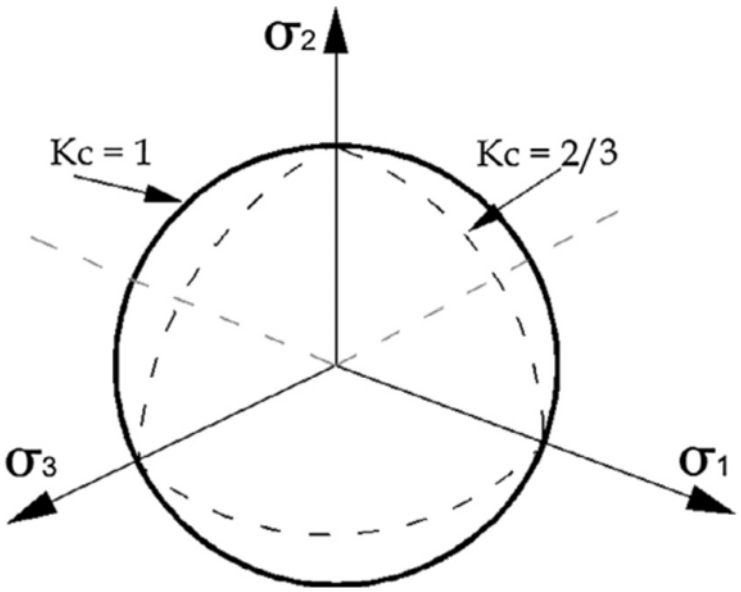

Figure 5. Yield surfaces in the deviatory plane ($K_c = \frac{2}{3}$ is related to Rankine formulation, $K_c = 1$ is corresponds to the Drucker-Prager law) [10].

Another parameter to define CPD (concrete plasticity damage) model is eccentricity that gives in the flow potential function approximation. It can be defined as Equation (5).

$$G(\sigma) = \sqrt{(\varepsilon\sigma_{t0}\tan\psi)^2 + \bar{q}^2} - \bar{p}\tan\psi, \tag{5}$$

where ε is the eccentricity, σ_{t0} is the uniaxial tensile stress and ψ is the dilation angle measured in the p-q plane [10]. The plastic potential function and yield surface are shown in Figure 6.

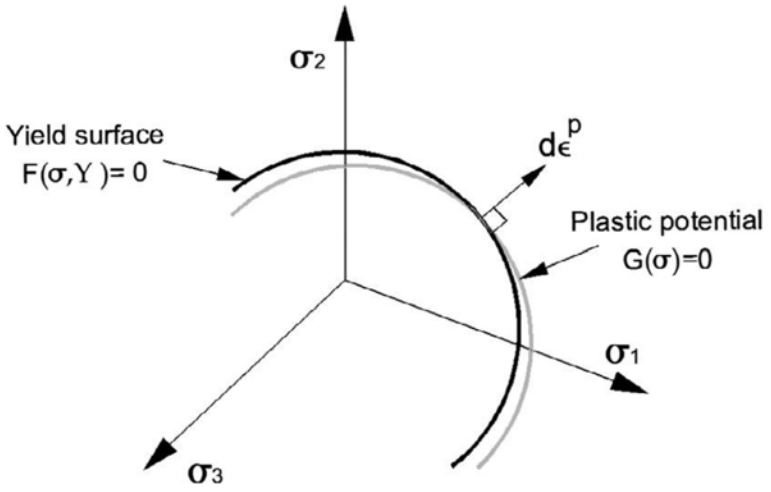

Figure 6. Plastic potential function and yield surface in the deviatoric plane [10].

The dilation angle shows the direction of plastic strain vector [16]. The dilation angle and eccentricity are depicted in Figure 7.

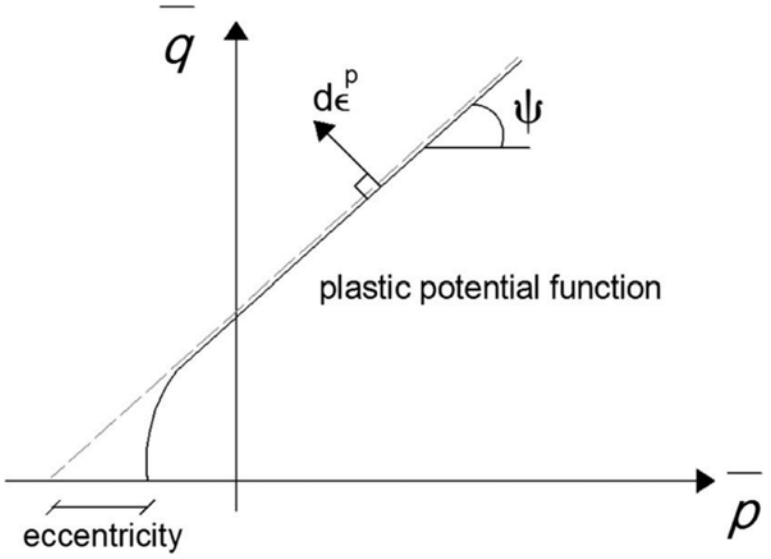

Figure 7. Dilation angle and eccentricity in meridian plane [10].

Viscoelasticity was modelled using Devaut-Lions approach. Damage model (d) is considered as follows:

$$\sigma = (1 - d)\overline{\sigma} = (1 - d)E_0 : (\in - \in^{pl}). \tag{6}$$

The strain rate with respect to the viscoplastic rate is defined in Equation (7):

$$\dot{\epsilon}_{\vartheta}^{pl} = \frac{1}{\mu}(\epsilon^{pl} - \epsilon_{\nu}^{pl}). \tag{7}$$

The viscoplastic damage is calculated as:

$$\dot{d}_{\nu} = \frac{1}{\mu}(d - d_{\nu}), \tag{8}$$

where d_{ν} is the stiffness degradation. So, the relation between stress and strain can be rewritten as follows:

$$\sigma = (1 - d)E_0 : (\epsilon - \epsilon_{\vartheta}^{pl}). \tag{9}$$

3. Material Properties

3.1. Concrete

The Poisson ratio was assumed to have a constant value for concrete damage plasticity model. The values of other parameters are reported in Table 2.

Table 2. The parameters used to simulate concrete damage plasticity (CDP) under compound stress

Parameter	Value
Dilation angle (ψ)	36
Eccentricity (ε)	0.1
σ_{b0}/σ_{c0}	1.16
K_c	0.667
Viscosity	0

The stress-strain curve based on Hognestad and Kent model [9] was used to define properties of concrete (Figure 8). The maximum stress was obtained about 85% of the cylindrical strength of the concrete which is related to 0.002 strain. The modulus of elasticity was given in the following equation for the linear part:

$$E_c = 12800 + 460 f_c \left(\mathrm{Kg}f / \mathrm{cm}^2\right). \tag{10}$$

The second part is given as a curvature shape which can be represented as:

$$\sigma_c = f_c \left[\frac{2\varepsilon_c}{\varepsilon_{c0}} - \left(\frac{\varepsilon_c}{\varepsilon_{c0}} \right)^2 \right]. \tag{11}$$

The ultimate compressive strain (ε_{cu}) can be achieved as 0.0038 for $0.85 f_c$.

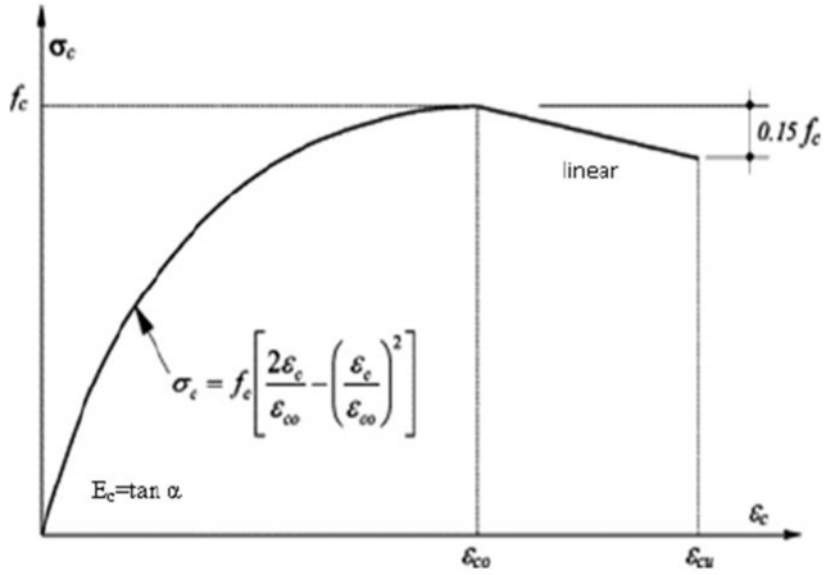

Figure 8. Stress-strain curve of Hognestad model [9].

Kent and Park [18] have proposed a new stress-strain curve for the behaviour of concrete which is shown in Figure 9.

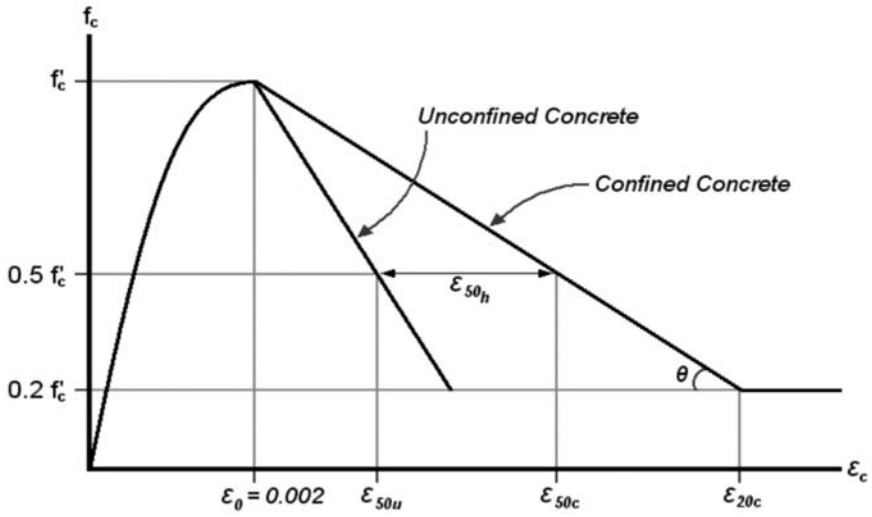

Figure 9. Stress-strain model for confined and unconfined concrete-Kent and Park model [18].

This model consists of two parts. The first part is modifying the parabolic part by replacing $f_c = f_{ck}$ and the second part can be presented as the following form:

$$\sigma_c = f_c\left[\frac{2\varepsilon_c}{0.002} - \left(\frac{\varepsilon_c}{0.022}\right)^2\right]. \tag{12}$$

The peak of the curve is assumed to be a straight line which the slope can be defined as a function of concrete strength [10]:

$$\sigma_c = f_c\{1 - Z(\varepsilon_c - 0.002)\}, \tag{13}$$

$$\varepsilon_{50u} = \frac{3 + 0.0285 f_c}{14.2 f_c - 1000}, \tag{14}$$

$$\varepsilon_{50h} = \frac{3}{4}\rho_s\sqrt{\frac{b}{s}}, \tag{15}$$

$$Z = \frac{0.5}{\varepsilon_{50u} + \varepsilon_{50h} - 0.002}, \tag{16}$$

where σ_c, b, and s are the concrete stress, the large size of the core concrete and stirrup spacing, respectively. Likewise, ρ_s is the percent density of stirrup that is given as:

$$\rho_s = \frac{A_{s0}(a+b)^2}{s(a)(b)}, \tag{17}$$

where a is the small size of the concrete. The mechanical behaviour of concrete was calculated by using different models (Table 3). The stress-strain hardening models for concrete are shown in Figure 10.

Table 3. The mechanical behaviour of concrete

Inelastic strain	Total strain	Kent & Park model	Hognestad model
	0	0	0
	0.0002	7562000	7562000
	0.0004	14328000	14328000
0	0.0006	20298000	20298000
0.0002	0.0008	25472000	25472000
0.0004	0.001	29850000	29801300
0.0006	0.0012	33432000	33432000
0.0008	0.0014	36218000	36218000
0.001	0.0016	38208000	38208000
0.0012	0.0018	39402000	39402000
0.0014	0.002	39800000	39136666.67
0.0016	0.0022	39402000	38473333.33
0.0018	0.0024	38208000	37810000
0.002	0.0026	36218000	37146666.67
0.0022	0.0028	33432000	36483333.33
0.0024	0.003	29850000	35820000
0.0026	0.0032	25472000	35156666.67
0.0028	0.0034	20298000	35156666.67
0.003	0.0036	14328000	34493333.33
0.0032	0.0038	7562000	34493333.33

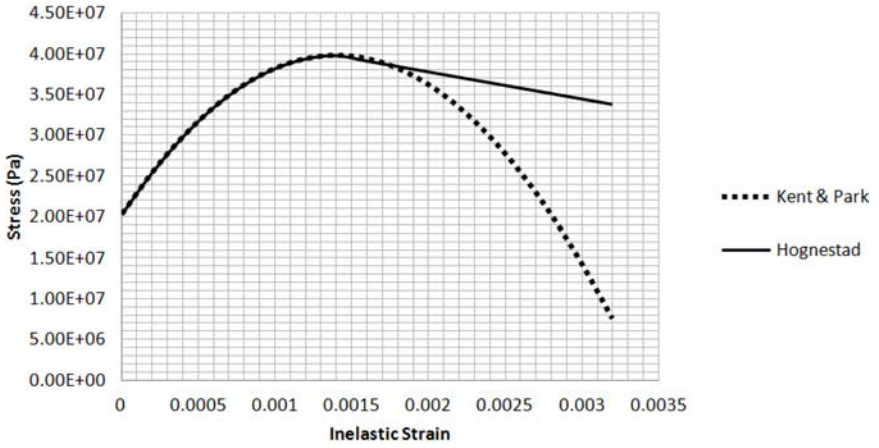

Figure 10. Stress-strain curve for Kent and Park model with a certain axial force.

There are several different failure modes in the CFRPs namely fiber rupture under tension, fiber buckling under tension and compression, matrix cracking under transverse tension and shearing. The mechanical properties of concrete are given in Table 4, where f_c is the compressive force, E is the elastic modulus and f_t is the tensile strength, ε_t is the strain, and P is the axial force.

Table 4. The behaviour of concrete (tensile and compressive strength)

Compressive force (f_c, MPa)	Elastic modulus (E, MPa)	Tensile strength		Axial force	
		f_t(MPa)	ε_t	Axial force ratio	P(MPa)
39,800	32174.4930	3.98	0.00001237	0.20	8.00
		0.0398	0.0001270		

3.2. CFRP

The elastic-plastic behaviour under static and dynamic loading was reported in previous studies [5, 19]. The failure of CFRP layers was analyzed using elastic material lamina by "Hashin" theory [12].

3.3. Adhesive

The adhesive layers were placed between the CFRP-metal interlayers. The epoxy adhesive response was applied using cohesive element and traction-separation law. The stress failure of the adhesive zone based on traction separation law was defined as Equation (18):

$$\left(\frac{t_n}{N}\right)^2 + \left(\frac{t_s}{S}\right)^2 + \left(\frac{t_t}{T}\right)^2 = 1, \tag{18}$$

where t_n, t_s, and t_t are the traction vector of normal stress, first and second direction of the adhesive layer [10]. Also N, S, and T are the maximum normal, shear stresses, and the directions, respectively.

In the present study, three series of CFRP beams A_4, B_4, C_4 [1] were used for numerical simulation. The material properties of steel for all series are given in Table 5.

Table 5. The mechanical properties of steel for all series [1]

Property	Materials					
	Series A		Series B		Series C	
	R_6	T_{10}	R_{12}	T_{20}	R_{16}	T_{32}
Yield stress (MPa)	348	547	324	544	324	552
Yield strain	0.17	0.35	0.17	0.35	0.20	0.45
Ultimate stress (MPa)	460	584	448	644	492	650
Modulus (GPa)	237	180	199	183	188	181

Moreover, the properties of CFRP, steel, concrete and adhesive sections used in the present research are reported in Table 6.

Table 6. The used material properties for simulation FEA [1]

Type of material	Parameters	Value
Steel	$\rho_s(\mathrm{kg/m^3})$	7800
	ϑ	0.3
Concrete	$\rho_s(\mathrm{kg/m^3})$	2400
	ϑ	0.15
CFRP	$E_{\mathrm{CFRP}}(\mathrm{GPa})$	235
	f^t_{CFRP}	3350
	$\varepsilon^t_{\mathrm{CFRP}}(\mathrm{Gpa})$	0.015
	$t_{\mathrm{CFRP}}(\mathrm{mm})$	0.165
Adhesive	$E_a(\mathrm{GPa})$	1824
	$G_a(\mathrm{MPa})$	622
	$t_a(\mathrm{mm})$	0.636

4. Validation of the FE Model

The FE results of bending failure of CFRP beams were compared with the experimental results [1] to validate the present FEM. This comparison was performed in terms of static loading vs. lateral displacement and plastic failure modes. The finite element model with the different number of total elements (2940, 5971, and 12829) was used for this process (Figure 11) and the sensitivity analysis of mesh was carried out as demonstrated in Figure 12.

(1) (2) (3)

Figure 11. FE model with different number of total elements to simulate concrete (1) 2940 Elements, (2) 5971 Elements, and (3) 12829 Elements.

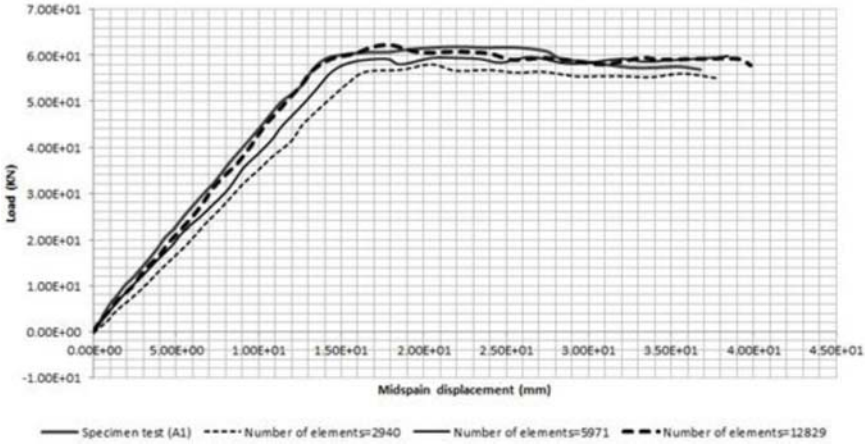

Figure 12. Mesh convergence graph.

According to the convergence graph (Figure 12), it is shown that the results do not change significantly by selecting the number of elements about 12829. Therefore, the third case was chosen as the optimal FEM to use on the future studies.

5. Results and Discussion

The three types of specimens (A, B, and C) were used to experimental study of the failure of CFRP beams. And five tests were performed for each group to consider repeatability. The finite element analysis was done with the same conditions of the experimental study. The stress contour of S_{11} and the damage zone in terms of plasticity are illustrated in Figure 13.

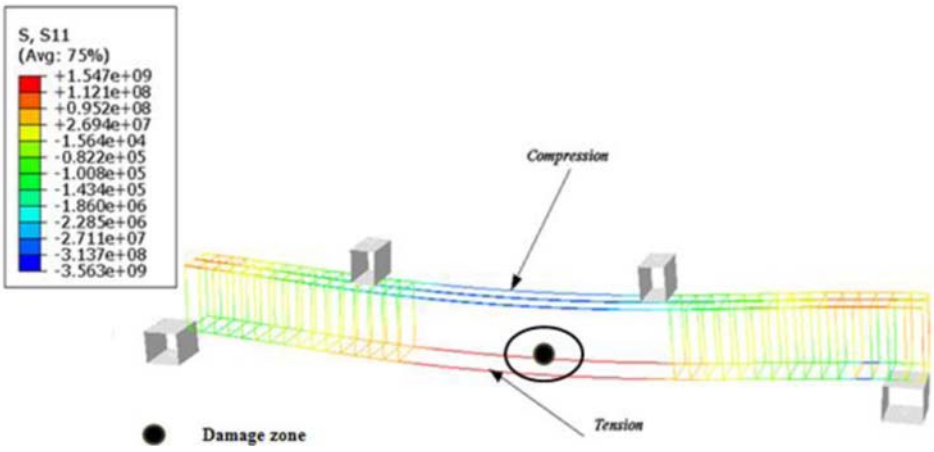

Figure 13. The stress contour of S_{11} and the damaged zone in terms of plasticity for specimen type A.

After that, the obtained finite element results were compared with experimental data as shown in Figure 14. The linear regression for numerical and experimental results was calculated for this sample. The maximum load in the damaged zone was equal to 7.38×10^{1}KN and 7.1×10^{1}KN for FE and experimental results, respectively.

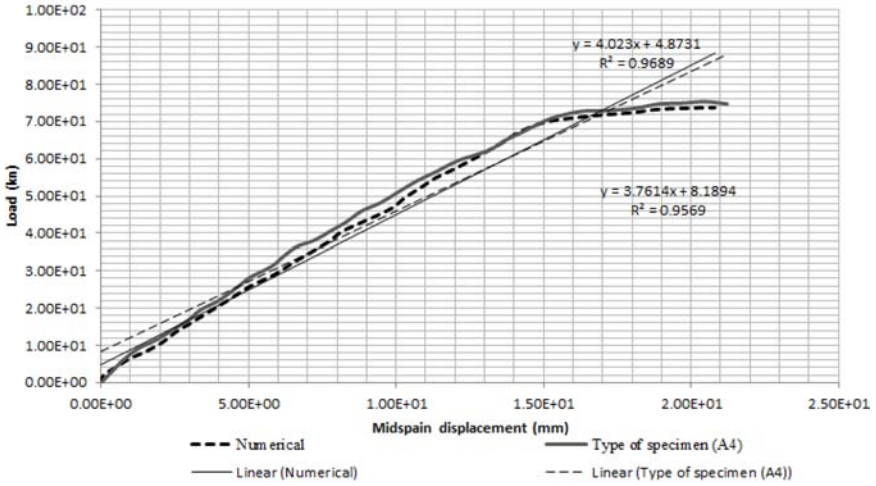

Figure 14. The load-displacement curves for numerical and experimental results.

The length and load of the specimen were changed for the case of B and the stress contour in the elastic-plastic state is presented in Figure 15.

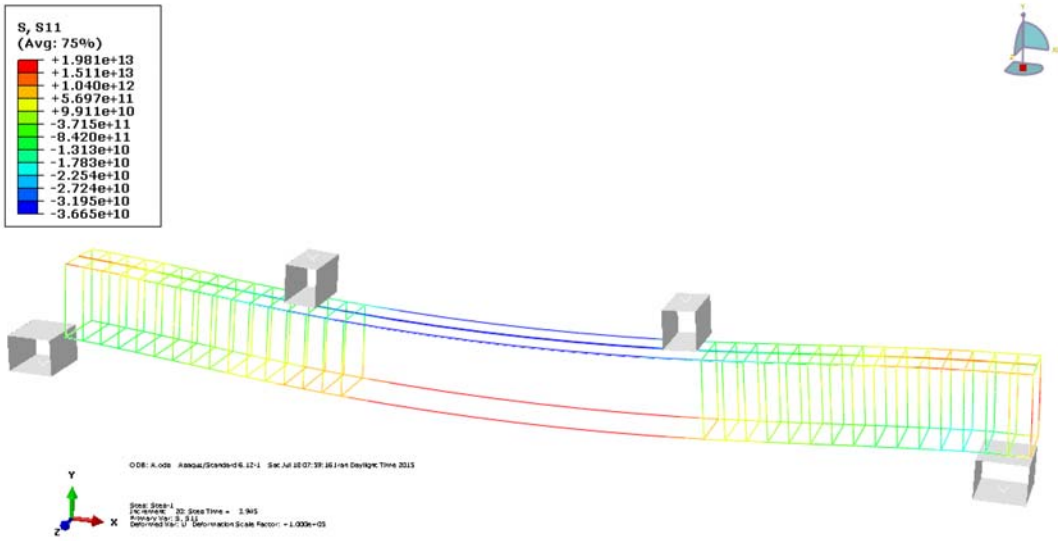

Figure 15. The stress contour of S_{11} for specimen type B of CFRP beam.

The deflection at the center of the specimen was obtained as the max value due to symmetrical conditions such as loading, geometry and etc. The yield load $(2.4\times10^{2}\mathrm{KN})$ was observed in the maximum deflection for the series of B. The load-displacement diagram for the case of B specimen is shown in Figure 16.

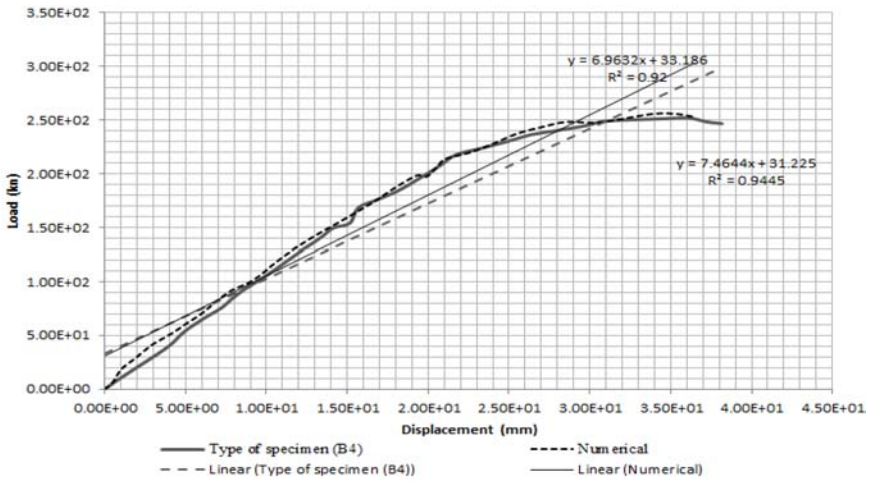

Figure 16. Numerical results for B series of CFRP beam.

The stress contour of S_{11} for the C type of CFRP beam is shown in Figure 17. The maximum principal stress of $S_{11} = 1.142 \times 10^{14}$ Pa was calculated in the damage zone for this type of beam. The maximum loading of 6.33×10^{2} KN was obtained with the displacement of 5.52×10^{1} mm in the failure region.

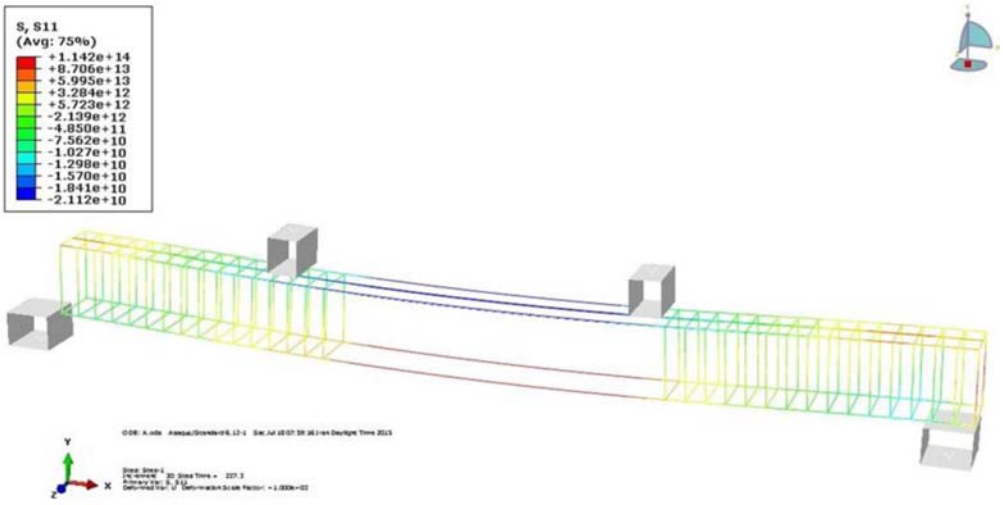

Figure 17. The stress contour of S_{11} for the series C of CFRP beam.

6. Conclusion

In the present paper, the bending failure of CFRP beams was studied using finite element simulation and experimental data. Three CFRP beams with different sizes and constant thickness by considering concrete damage plasticity model were used to simulate FEM. The obtained FEM results were in a good agreement with the experimental data. The main findings of the present study can be summarized as:

(1) The obtained FE results were in a good agreement with experimental data. Therefore, the FEM presented in this study had a good accuracy and it can be used for different applications.

(2) The present finite element model can successfully predict the maximum stress and deflection in the failure region in terms of plasticity.

(3) The proposed simulation can be effectively used to predict the static and failure responses of the CFRP beams.

References

[1] M. Maalej and K. S. Leong, Effect of beam size and FRP thickness on interfacial shear stress concentration and failure mode of FRP-strengthened beams, Composites Science and Technology 65(7-8) (2005), 1148-1158.

DOI: https://doi.org/10.1016/j.compscitech.2004.11.010

[2] H. Sezen, A. S. Whittaker, K. Elwood and K. Mosalam, Performance of reinforced concrete buildings during the August 17, 1999 Kocaeli, Turkey earthquake, and seismic design and construction practice in Turkey, Engineering Structures 25(1) (2003), 103-114.

DOI: https://doi.org/10.1016/S0141-0296(02)00121-9

[3] S. Tabrizi, H. Kazem, S. Rizkalla and A. Kobayashi, New small-diameter CFRP material for flexural strengthening of steel bridge girders, Construction and Building Materials 95 (2015), 748-756.

DOI: https://doi.org/10.1016/j.conbuildmat.2015.07.109

[4] H. M. Ali, A. Iqbal and L. Liang, A comparative study on the use of drilling and milling processes in hole making of GFRP composite, Sadhana 38(4) (2013), 743-760.

DOI: https://doi.org/10.1007/s12046-013-0186-5

[5] M. I. Alam, S. Fawzia and X. Liu, Effect of bond length on the behaviour of CFRP strengthened concrete-filled steel tubes under transverse impact, Composite Structures 132 (2015), 898-914.

DOI: https://doi.org/10.1016/j.compstruct.2015.06.065

[6] B. Almassri, J. A. O. Barros, F. Al Mahmoud and R. Francois, A FEM-based model to study the behaviour of corroded RC beams shear-repaired by NSM CFRP rods technique, Composite Structures 131 (2015), 731-741.

DOI: https://doi.org/10.1016/j.compstruct.2015.06.030

[7] H. Jiang and M. G. Chorzepa, An effective numerical simulation methodology to predict the impact response of pre-stressed concrete members, Engineering Failure Analysis 55 (2015), 63-78.

DOI: https://doi.org/10.1016/j.engfailanal.2015.05.006

[8] N. T. Khshain, R. Al-Mahaidi and K. Abdouka, Bond behaviour between NSM CFRP strips and concrete substrate using single-lap shear testing with epoxy adhesive, Composite Structures 132 (2015), 205-214.

DOI: https://doi.org/10.1016/j.compstruct.2015.04.060

[9] E. Hognestad, Ultimate strength of reinforced concrete in American design practice, Proceedings S2 1 (1956), 12SS.

[10] A. S. Genikomsou and M. A. Polak, Finite element analysis of punching shear of concrete slabs using damaged plasticity model in ABAQUS, Engineering Structures 98 (2015), 38-48.

DOI: https://doi.org/10.1016/j.engstruct.2015.04.016

[11] I. Jankowiak, W. Kakol and A. Madaj, Identification of a continuous composite beam numerical model, based on experimental tests, in 7th Conference on Composite Structures, Zielona Góra (2005), 163-178.

[12] Z. Hashin, Failure criteria for unidirectional fiber composites, Journal of Applied Mechanics 47(2) (1980), 329-334.

DOI: https://doi.org/10.1115/1.3153664

[13] Z. Hashin and A. Rotem, A fatigue failure criterion for fiber reinforced materials, Journal of Composite Materials 7(4) (1973), 448-464.

DOI: https://doi.org/10.1177/002199837300700404

[14] A. Faggiani and B. Falzon, Predicting low-velocity impact damage on a stiffened composite panel, Composites Part A: Applied Science and Manufacturing 41(6) (2010), 737-749.

DOI: https://doi.org/10.1016/j.compositesa.2010.02.005

[15] Y. Shi, T. Swait and C. Soutis, Modelling damage evolution in composite laminates subjected to low velocity impact, Composite Structures 94(9) (2012), 2902-2913.

DOI: https://doi.org/10.1016/j.compstruct.2012.03.039

[16] ABAQUS, Analysis User's Manual 6.14-EF, Dassault Systems Simulia Corp., Providence, RI, USA, 2015.

[17] J. Lee and G. L. Fenves, Plastic-damage model for cyclic loading of concrete structures, Journal of Engineering Mechanics 124(8) (1998), 892-900.

DOI: https://doi.org/10.1061/(ASCE)0733-9399(1998)124:8(892)

[18] D. C. Kent and R. Park, Flexural members with confined concrete, Journal of the Structural Division 97(7) (1971), 1969-1990.

[19] S. Fawzia, R. Al-Mahaidi, X. L. Zhao and S. Rizkalla, Strengthening of circular hollow steel tubular sections using high modulus CFRP sheets, Construction and Building Materials 21(4) (2007), 839-845.

DOI: https://doi.org/10.1016/j.conbuildmat.2006.06.014

■